Correlating DFT Calculations with CO Oxidation Reactivity on Ga-Doped Pt/CeO2 Single-Atom Catalysts

Yingxin Feng,[†] Qiang Wan,[†] Haifeng Xiong,*,[‡] Shulan Zhou,[§,‖] Xun Chen,[†]
Xavier Isidro Pereira Hernandez,[⊥] Yong Wang,[⊥,#] Sen Lin,*,[†,§] Abhaya K. Datye,*,[‡]
and Hua Guo*,[§]

[†]State Key Laboratory of Photocatalysis on Energy and Environment, College of Chemistry, Fuzhou University, Fuzhou 350002, China

[‡]Center for Microengineered Materials, Department of Chemical & Biological Engineering and [§]Department of Chemistry and Chemical Biology, University of New Mexico, Albuquerque, New Mexico 87131, United States

[‖]Department of Material Science and Engineering, Jingdezhen Ceramic Institute, Jingdezhen 333403, Jiangxi, China

[⊥]Voiland School of Chemical Engineering and Bioengineering, Washington State University, Pullman, Washington 99164, United States

[#]Institute for Integrated Catalysis and Environmental Molecular Sciences Laboratory, Pacific Northwest National Laboratory, P.O. Box 999, Richland, Washington 99352, United States

Ⓢ *Supporting Information*

ABSTRACT: Pt/CeO_2 single-atom catalysts have recently attracted increasing interest due to excellent thermal stability, high atom efficiency, and high activity in catalysis. In this study, by means of density functional theory (DFT) calculations, we systematically compare the stability and CO oxidation reactivity of Pt single atoms supported on $CeO_2(111)$ (Pt/CeO_2) and Ga-doped $CeO_2(111)$ ($Pt/Ga-CeO_2$). It was found that the formation of an oxygen vacancy (O_V) is very facile near a surface Ga-doping site ($Pt/Ga-CeO_2-O_V$). Significantly, the stability of Pt single atoms anchored on the Ga site was enhanced compared with those on the bare ceria surface. In addition, our DFT results suggest a CO oxidation mechanism on $Pt/Ga-CeO_2-O_V$ that differs from that on Pt/CeO_2. In particular, the O_V site plays an important role in activating the oxygen molecule, which then reacts with CO preadsorbed on Pt. The calculated energy barrier on $Pt/Ga-CeO_2-O_V$ is about 0.43 eV lower than that on the undoped catalyst, suggesting an enhanced reactivity for CO oxidation. Experiments on CO oxidation and in situ diffuse reflectance infrared Fourier transform spectroscopy are performed to corroborate the results obtained from the DFT calculations, and a good agreement is achieved. The combination between calculations and experiments sheds light on the influence of support doping on atomically dispersed Pt/CeO_2 catalysts.
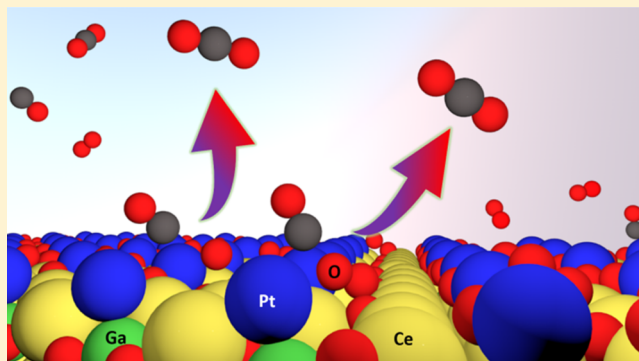
1. INTRODUCTION

Single-atom catalysis, in which chemical transformation is accelerated by atomically dispersed metal atoms on supports, has attracted ever-increasing attention because of their atom efficiency and unique reactivity and selectivity.[1−9] One issue in this emerging field is that the dispersed metal atoms tend to sinter under high-temperature reaction conditions, resulting in the formation of nanoparticles leading to altered catalytic activity.[10] To prevent/minimize agglomeration of single metal atoms under reaction conditions, numerous studies have to be carried out to identify supports that can provide surface sites to strongly trap single metal atoms. Such sites have been found on, for example, FeO_x,[11] γ-Al_2O_3,[12] and the (111) surface of $MgAl_2O_4$ for binding Pt in the form of nanoclusters or isolated atoms.[13] However, when temperature is increased to ca. 800

°C, the formation of large Pt nanoparticles is detected via X-ray diffraction, indicating the onset of sintering.[13,14]

CeO_2 is one of the most attractive supports due to its unique redox and acid/base properties and the ability to stabilize metal particles or trap single atoms.[15−17] Some of the current authors previously reported that CeO_2 has the unique ability to trap Pt single atoms and to resist Pt sintering at elevated temperatures (i.e., 800 °C) under oxidizing conditions.[18] The resulting Pt/CeO_2 single-atom catalyst (SAC) showed comparable specific reactivity in CO oxidation as conventional supported Pt or Pt single crystal model catalysts.[18] After steam

treatment, the Pt/CeO$_2$ SAC was shown to present improved activity in exhaust catalysis due to the activation of surface lattice oxygens.[19] Although Pt/CeO$_2$ SACs demonstrate high stability, they provide poor selectivity during catalytic propane dehydrogenation at 680 °C.[15] To improve the propylene selectivity, we added Sn metal atoms into the lattice of the CeO$_2$ substrate to modify the performance of the Pt/CeO$_2$ SAC. We found that the doping of Sn atoms significantly enhances the propylene selectivity in propane dehydrogenation by tuning the electronic structures of the Pt atoms on the doped CeO$_2$ support, which was confirmed by density functional theory (DFT) calculations.[15] Further studies are needed to understand the influence of hetero-metal dopants to modify the structure and performance of Pt/CeO$_2$ SACs in catalysis.

In this work, we explore the stability and CO oxidation activity of Pt SACs supported on bare and Ga-doped CeO$_2$(111) (denoted respectively as Pt/CeO$_2$ and Pt/Ga−CeO$_2$), using periodic DFT computation. Our calculation results show that the replacement of a surface Ce atom on the CeO$_2$(111) surface by a Ga atom promotes the formation of an oxygen vacancy (O$_V$) nearby. A Pt atom can then bind strongly with the Ga dopant on the surface, thus forming a stable SAC for CO oxidation. The calculation results further suggest that Ga doping leads to superior catalytic performance for CO oxidation with a different reaction mechanism than that on Pt/CeO$_2$. To verify the theoretical predictions, we conducted experiments on the kinetics of the CO oxidation catalyzed by Pt/Ga−CeO$_2$ with an oxygen vacancy. The experimental results are found to be consistent with the DFT calculations. The combined results from the DFT calculations and experiment provide important insights for developing thermally stable and active metal-doped Pt SACs on ceria.

2. METHODS

2.1. Computational Method. All the calculations were based on periodic DFT and carried out using the Vienna ab initio simulation package[20−22] with the PW91 functional. To accurately describe the highly localized Ce 4f-orbitals, we performed spin-polarized DFT + U calculations with a value of U = 4.5 eV applied to the Ce 4f states, following previous theoretical studies.[23] The electronic wave function was expanded in plane waves up to a cutoff energy of 400 eV[24,25] and the ionic core electrons were approximated by the projector augmented wave method.[26] The calculated CeO$_2$ lattice parameter of 5.44 Å is consistent with the previously reported experimental and theoretical values.[27,28] The doped CeO$_2$ system was simulated by replacing one lattice Ce atom on the topmost layer with a Ga atom (denoted as Pt/Ga−CeO$_2$). The slabs were modeled with nine atomic layers containing a 2 × 2 unit cell. During geometry optimization, the atoms in the top six atomic layers and the adsorbates were fully relaxed until the force acting on each atom was less than 0.05 eV/Å, whereas other atoms were fixed. To avoid the artificial interactions along the z-direction between its periodic images, a vacuum space with a length of 14 Å was employed. A 2 × 2 × 1 k-point mesh was adopted to sample the Brillouin zone, which is tested to be converged.

The formation energy of oxygen vacancy (O$_V$) is calculated as $E_f = E(\text{slab-O}_V) − E(\text{slab}) + 1/2E(O_2)$, where $E(\text{slab})$ is the energy of the perfect supercell and $E(\text{slab-O}_V)$ is the energy of the supercell with an oxygen vacancy. The adsorption energy E_{ads} is defined by $E_{ads} = E_{(\text{adsorbate−catalyst})} − E_{\text{adsorbate}} − E_{\text{catalyst}}$,

where $E_{\text{adsorbate}}$ is the energy of free adsorbate species, E_{catalyst} is the energy of the catalyst, and $E_{(\text{adsorbate−catalyst})}$ is the total energy of the complex.

The formation energy of the Ga (E_f) substituted surface was calculated using the following equation

$$\text{Ga(s)} + \text{Ce}_x\text{O}_{2x}(\text{surf}) + \text{O}_2(\text{g})$$
$$\rightarrow \text{Ga−Ce}_{x−1}\text{O}_{2x}(\text{surf}) + \text{CeO}_2(\text{s})$$
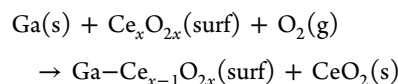
The climbing image nudged elastic band (CI-NEB)[29] approach was employed to simulate CO oxidation on the SACs, generating the reaction path. The activation barrier E_a for each reaction step was calculated as the energy difference between the transition state and the initial state, whereas the reaction energy ΔE for each reaction step was calculated as the energy difference between the final state and the initial state. The convergence of relaxation was checked with a 0.05 eV/Å criterion.

2.2. Experimental Method. *2.2.1. Catalyst Preparation.* The Pt/CeO$_2$ SAC was prepared by the method reported in our previous work.[15,18,19] Briefly, Ce(NO$_3$)$_3$·6H$_2$O (99.999%; Sigma-Aldrich) was heated in air at 350 °C for 2 h to obtain CeO$_2$ polyhedra (Brunauer−Emmett−Teller surface area: ca. 68 m^2/g). The Pt/CeO$_2$ catalyst (1 wt % Pt, nominal) was prepared by incipient wetness impregnation. An appropriate amount of chloroplatinic acid (Sigma-Aldrich, 8 wt %) was added dropwise to CeO$_2$ under continuous stirring. The powder was then dried at 120 °C for 12 h. Afterward, the sample was directly calcined and thermally aged at 800 °C for 12 h in flowing air. The formed sample is designated as Pt/CeO$_2$, which has been extensively characterized as described in our earlier publication.[18] The Ga-doped Pt/CeO$_2$ catalyst (1 wt % Pt, Pt/Ga atomic ratio = 1) was prepared by the similar impregnation method. First, an appropriate amount of Ga(NO$_3$)$_3$ solution was impregnated into the as-prepared CeO$_2$ support. Then, the material was dried at 120 °C for 12 h, followed by calcination at 500 °C for 6 h in air. After that, an appropriate amount of chloroplatinic acid (Sigma-Aldrich, 8 wt %) was added dropwise to the Ga-doped CeO$_2$ under continuous stirring. The powder was then dried at 120 °C for 12 h. Afterward, the sample was directly calcined and thermally aged at 800 °C for 12 h in flowing air (similar procedure as Pt/CeO$_2$). The obtained sample is designated as Pt/Ga−CeO$_2$.

2.2.2. Diffuse Reflectance Infrared Fourier Transform Spectroscopy (DRIFTS). Diffuse reflectance infrared Fourier transform spectroscopy (DRIFTS) measurements were performed on an IR spectrometer Tensor 27 from Bruker, coupled with a Praying Mantis Diffuse Reflection accessory from Harrick. A ThermoStar GSD 320 T quadrupole mass spectrometer from Pfeiffer Vacuum with a Secondary Electron Multiplier was connected to monitor the outlet flow composition. The spectra and backgrounds taken had a resolution of 4 cm^{-1} and 128 scans were averaged for each spectrum and background. The detailed DRIFTS experimental procedures can be found in our previous work.[18] Briefly, the catalyst was pretreated at 300 °C for 0.5 h under 10% O$_2$/He (40 sccm) and purged with helium for 0.5 h (40 sccm) at the same temperature. The temperature was then decreased to 125 °C and a background spectrum was taken. One percent CO and 10% O$_2$ balanced with He were introduced into the cell at a flow rate of 40 sccm for 30 min. Afterward, the flow of CO
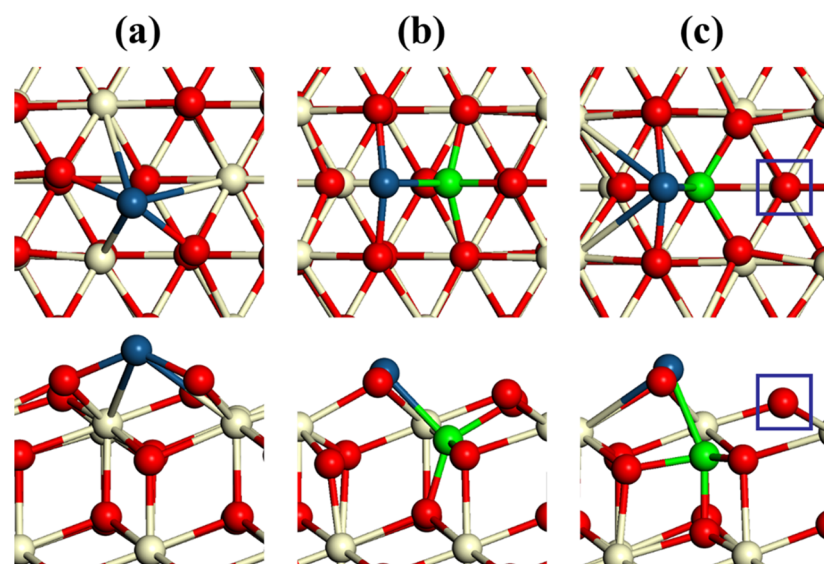
Figure 1. Top view (upper panels) and side view (lower panels) of (a) Pt−CeO$_2$ and (b) Pt/Ga−CeO$_2$ and (c) Pt/Ga−CeO$_2$−O$_V$. The O$_V$ is indicated by a square frame. Color scheme: Pt, blue; Ga, green; Ce, yellow; O, red.

was discontinued and O$_2$ or He was kept flowing for 10 min while the spectra were recorded.

2.2.3. CO Oxidation. The CO oxidation experiments were performed in a quartz tube fixed-bed reactor (OD = 1/4 inch), and the gases (CO, O$_2$, and CO$_2$) were analyzed using an Agilent 490 Micro-GC utilizing a TCD detector. The powder samples (60 mg) were packed between quartz wool with a thermocouple placed touching the sample inside the reactor. The CO oxidation conditions used were 1.5 mL/min CO, 1 mL/min O$_2$, and 75 mL/min He, with a ramp rate of 2 °C/min and sampling performed every 3 min.

3. RESULTS AND DISCUSSION

3.1. Geometries and Stability of SACs. Among all the possible facets, the O-terminated CeO$_2$(111) surface is considered as the most stable because it has the lowest surface energy.[30] It is known to provide various adsorption sites for Pt atoms.[31,32] In addition, doping of hetero-metal atoms into the CeO$_2$ lattice has emerged as a useful route to promote the interaction between the metals and the CeO$_2$(111) surface.[33,34]

On bare CeO$_2$(111), a Pt atom is found from our DFT calculations to adsorb at the hollow site (Figure 1a and denoted as Pt/CeO$_2$), consistent with the previous theoretical studies, in which the metal atoms were found to have the most stable states when they are loaded on the 3-fold hollow sites of CeO$_2$.[15,27,35] For the Ga-doped CeO$_2$, some Ce sites might be replaced with Ga near the surface (Figure 1b). The formation energy of the Ga−CeO$_2$ surface is found to be −2.39 eV, indicating that the Ga substitution into the Ce position is thermodynamically favored. The Pt atom prefers to bind to the surface Ga site because of a stronger interaction with Ga than with surface oxygens. Interestingly, we found that an oxygen vacancy (O$_V$) can be easily generated near the Ga site (Figure 1c) (denoted as Pt/Ga−CeO$_2$−O$_V$) with a calculated O$_V$ formation energy of merely 0.09 eV. The reason is that when a formally 4+ cation (Ce^{4+}) is substituted by formally 3+ cation (Ga^{3+}), the system will become unstable because the 3+ oxidation state of the dopant leads to the addition of one electron compared to the 4+ cation. The usual way to maintain

the charge balance is through the creation of an O vacancy, which can then activate the adsorbed oxygen molecule. However, the calculated formation energy of an oxygen vacancy is as high as 2.76 eV for Pt/CeO$_2$, thus ruling out the possibility of a stable oxygen vacancy. The lowering of oxygen vacancy formation energy by doping of CeO$_2$ has been well documented.[17] Considering the formation energies for the Ga−CeO$_2$ surface and O$_V$, it can be concluded that the Ga dopant and O$_V$ are likely to coexist.

The binding energies, Bader charges, and key geometrical parameters for the supported Pt atoms are listed in Table 1.

Table 1. Binding Energies (eV), Bader Charges (|e|), and Geometrical Parameters (Å) for the Supported Pt Atoms

	Pt/CeO$_2$(111)	Pt/Ga−CeO$_2$(111)−O$_V$
E_b/eV	−2.69	−4.67
Bader charge/|e|	+0.08	+0.24
d_{Pt-O}/Å	2.14	1.99
d_{Pt-Ga}/Å		2.45

Clearly, from the table, we can see significant differences among these catalysts. Doping of Ga into the CeO$_2$ lattice can greatly enhance the stability of Pt atoms on the CeO$_2$(111) support. On bare CeO$_2$(111), the adsorption energy of Pt is −2.69 eV. On Ga-doped CeO$_2$ with O$_V$, however, the adsorption energy of Pt is increased to −4.67 eV. As shown Table 1, by doping of Ga, the Pt SAC is formed with the Pt−Ga bond distance of 2.45 Å and the distance of Pt−O bonds equal to 1.99 Å.

Single metal atoms tend to agglomerate on support surfaces when the temperature is increased and the catalytic activity may be partly or totally lost.[36−38] To evaluate the stability of SACs, we calculated the energy barrier of the Pt atom migration from the most stable adsorption site to an adjacent oxygen bridge adsorption site. The NEB results show that on the bare CeO$_2$ surface, the diffusion of a Pt atom is facile because the calculated migration barrier is as low as 0.19 eV. This means that the Pt atoms on bare CeO$_2$(111) are not expected to be stable at high temperatures. This is supported

by our recent experimental observations in Pt/CeO$_2$ catalysis of propane dehydrogenation, where the scanning transmission electron microscopy images showed that isolated Pt coexists with Pt nanoclusters having an average size of about 1.1 nm in the Pt/CeO$_2$ after propane dehydrogenation at 680 °C.[15] Interestingly, as indicated by the experiment with Sn doping, atomically dispersed species, and subnanometer Pt clusters with a reduced average size of 0.6 nm were observed.[15] Such a change highlights the importance of doping of CeO$_2$ in improving the stability of single Pt atoms. For Ga on Pt/Ga−CeO$_2$−O$_V$, the calculated migration energy of Pt from the most stable oxygen bridge site with Ga to an adjacent oxygen bridge site is as high as +2.28 eV, indicating that the migration is difficult and the isolated Pt atoms could be anchored on CeO$_2$ with sufficient stability to resist aggregation under high temperatures.

3.2. Charge Transfer. To better understand the binding nature of the Pt-support interaction, a Bader charge analysis was carried out. As listed in Table 1, the supported Pt atoms possess positive charges of +0.24 and +0.08 |e| for Pt/Ga−CeO$_2$−O$_V$ and Pt/CeO$_2$, respectively. The significant electron transfer from Pt atoms to the support is likely relevant to the stabilization of these single atoms. The trend for the charge transfer is consistent with that for the stability of Pt on these two supports. Moreover, the positive Bader charges mean that the Pt atoms are in oxidized forms, which might promote the catalytic activity of CO oxidation or the other reactions,[1,32,39] and will be discussed below.

3.3. Adsorption of CO and O$_2$. CO oxidation is a prototypical heterogeneous catalytic reaction.[5,40,41] For this reason, it is chosen in this work as a probe to explore the catalytic activity of the Pt single atoms supported on CeO$_2$(111) with and without doping. We have tested all the possible adsorption configurations on the SACs to find out the most stable states for CO and O$_2$ (Figure 2), and the adsorption energies and the key structural parameters are summarized in Table 2.

On the Pt/CeO$_2$ SAC, CO adsorbs on the Pt atom with an end-on configuration. The adsorption energy (E_{ads} = −3.26 eV) is strong, which might cause poisoning of the SAC. It should also be noted that upon CO adsorption the Pt atom is pulled out of the adsorption site and connects to only one surface oxygen (Figure 2a), suggesting a significant weakening of the Pt−CeO$_2$ interaction. For the adsorption of CO on the Pt/Ga−CeO$_2$−O$_V$ SAC (Figure 2b), the most favorable configurations appear to be an end-on structure in which the O−C bond is almost perpendicular to the catalyst plane, which is similar to that on Pt/CeO$_2$. Interestingly, the interaction between the Pt atom and CO on Pt/Ga−CeO$_2$−O$_V$ is much weaker than that on the Pt/CeO$_2$ SAC, with the E_{ads} value equal to −2.22 eV. More importantly, the Pt atom remains in its initial position, keeping the strong bonding with three surface oxygen atoms. The bond lengths of the adsorbed CO species are 1.16 Å, slightly elongated from its isolated state (1.14 Å), indicating minimal perturbation of its electronic structure after adsorption on the Pt atom.

The O$_2$ molecule is found to adsorb on the Pt atom on the Pt/CeO$_2$(111) SAC (Figure 2a), with the O−O bond length of 1.38 Å, yielding a moderate binding energy of −1.42 eV. The elongation of the O−O bond by 0.14 Å indicates that the adsorbed O$_2$ molecule is activated by the Pt SAC. Meanwhile, the Pt atom is also somewhat pulled out from its initial position with the two Pt−O distances of 2.12 Å, similar to the
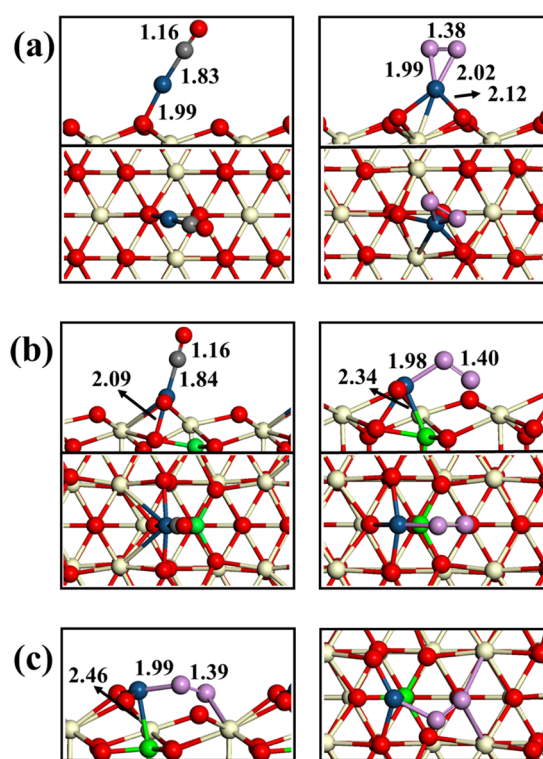
Figure 2. Side and top views of the optimized structures of CO and O$_2$ adsorbed on the Pt atoms of (a) Pt/CeO$_2$, (b) Pt/Ga−CeO$_2$−O$_V$, and (c) O$_2$ adsorbed at O$_V$ site of Pt/Ga−CeO$_2$−O$_V$. Color scheme: Pt, blue; Ga, green; Ce, yellow; O, red; O in O$_2$ molecule, purple.

Table 2. Adsorption Energies (E_{ads}, eV) of CO/O$_2$ on the Pt Atom Sites and the Relevant Key Geometrical Parameters (Å)^a

	Pt/CeO$_2$	Pt/Ga−CeO$_2$−O$_V$
	CO	
E_{ads}/eV	−3.26	−2.22
$d_{C−O}$/Å	1.16	1.16
$d_{M−C}$/Å	1.83	1.84
	O$_2$	
E_{ads}/eV	−1.42	−1.13
$d_{O−O}$/Å	1.38	1.39
$d_{M−O}$/Å	1.99, 2.02	1.99

^{a}The corresponding structures are shown in Figure 2.

case for CO adsorption. On the Pt/Ga−CeO$_2$−O$_V$ SAC, O$_2$ can adsorb at the Pt atom with one of its oxygen and the calculated O−O bond length is about 1.40 Å (Figure 2b), yielding a binding energy of −1.45 eV, which is comparable to that without doping. Obviously, the interaction between O$_2$ and the Pt atom is much weaker than that between CO and the Pt atom. In addition, the calculation results indicate that these two species, i.e., O$_2$ and CO, cannot coadsorb on the Pt site after extensive structural optimization. Therefore, O$_2$ has to adsorb at the O$_V$ site near the Pt atom (Figure 2c), with the binding energies of −1.13 eV and the O−O bond length of 1.39 Å for the Pt/Ga−CeO$_2$−O$_V$ SAC.

As indicated in the previous DFT studies that the activation of O$_2$ is the most important step of CO oxidation,[5,42−45] we carried out charge density difference (CDD) calculations to obtain a deeper understanding of the interaction of the O$_2$ molecule with the Pt atom in the Pt/CeO$_2$ SAC and with the
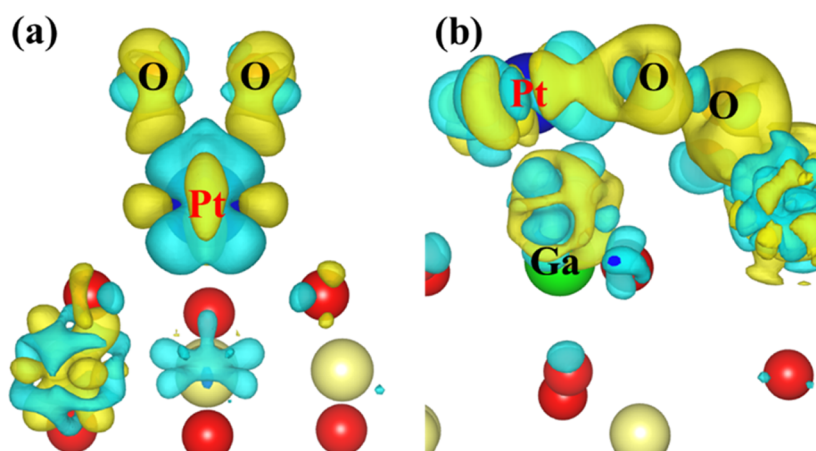
Figure 3. Contour plots of differential charge densities of O_2 absorbed on (a) Pt/CeO_2 and (b) $Pt/Ga-CeO_2-O_V$. The charge accumulation region is rendered in yellow, whereas the charge depletion region is in blue. The isosurface level is 0.0075 au. Color scheme: Pt, dark blue; Ga, green; Ce, yellow; O, red.
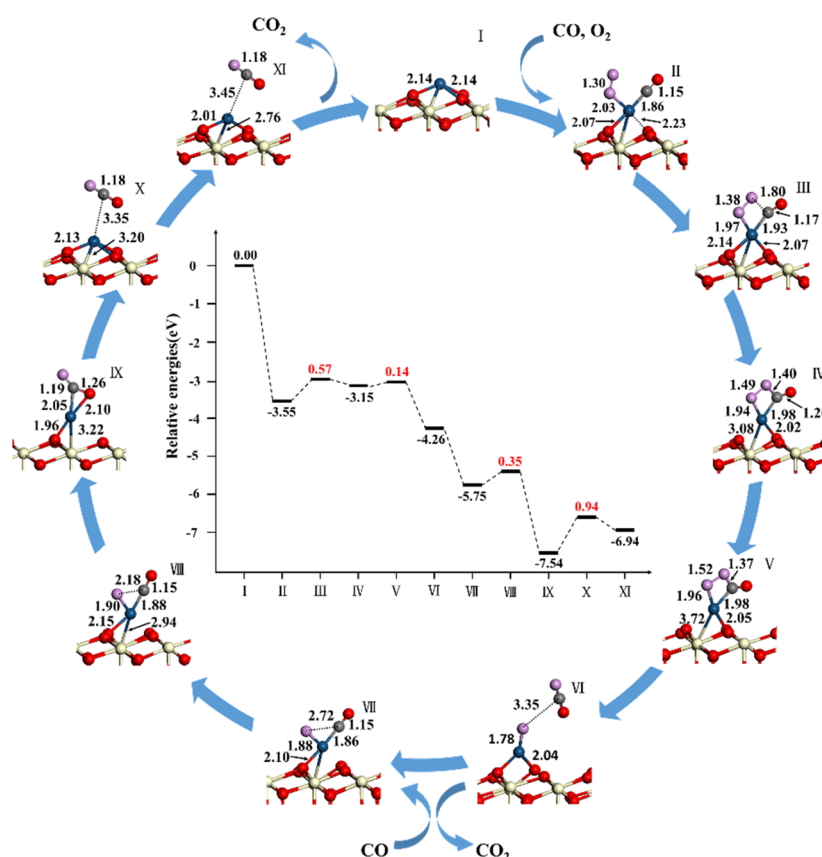
Figure 4. Reaction pathways of CO oxidation on Pt/CeO_2. Color scheme: Pt, blue; Ce, yellow; O, red; O in O_2 molecule, purple.

oxygen vacancy on the $Pt/Ga-CeO_2-O_V$ SAC. As displayed in Figure 3, the calculated CDD reveals that significant charge is transferred from the Pt/CeO_2 and $Pt/Ga-CeO_2-O_V$ SACs to the adsorbed O_2. The excess charge accumulate at the O−O bond region and fill into the $2\pi^*$ antibonding orbital of the O_2 molecule, resulting in the observed elongation of the O−O bond length.

3.4. Mechanism of CO Oxidation. Previous experimental and theoretical studies indicated that CO oxidation can take place on doped or undoped CeO_2.[23,25,35] Particularly, considering the low oxygen vacancy formation energies on $Pt/CeO_2(110)$, CO species tend to react with lattice oxygen to generate CO_2,[39] following the Mars−van Krevelen (MvK) mechanism. To find out whether CO oxidation can take place following this mechanism, we calculated the reaction energies (ΔE) of CO oxidation (CO abstracts a lattice oxygen, which connects to Pt to produce CO_2). The values are 2.16 eV on $Pt/CeO_2(111)$, indicating that the MvK pathway is thermodynamically unfavorable on this SAC and therefore not considered further.

To gain insights into the catalytic activity of the CeO_2-supported Pt SACs, the NEB method is used to calculate the energy barriers for CO oxidation. The reaction pathways with
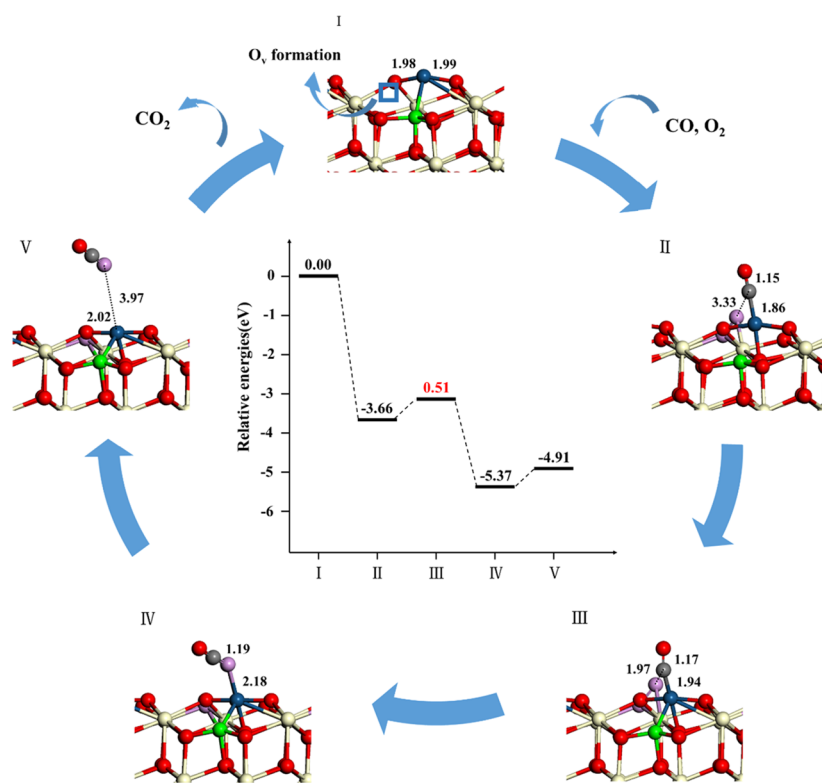
Figure 5. New reaction pathway of CO oxidation on Pt/Ga−CeO$_2$−O$_V$. The O$_V$ is indicated by a square frame. Color scheme: Pt, blue; Ga, green; Ce, yellow; O, red; O in O$_2$ molecule, purple.

energy barriers (E_a) of CO oxidation on these two SACs are shown in Figures 4 and 5, respectively.

As shown in Figure 4 for the Pt/CeO$_2$ SAC, in the initial state (II), both CO and O$_2$ coadsorb on the Pt atom with the O−O and C−O bond lengths of 1.30 and 1.15 Å, respectively. In the transition state (III), one O atom of the adsorbed O$_2$ moves closer to the C atom with a distance of 1.80 Å. Meanwhile, the O−O and C−O bond lengths are elongated to 1.38 and 1.17 Å, respectively. The first reaction step generates an intermediate (IV), in which the O$_2$ connects to the C and Pt atoms to form a four-member circle with O−O, O−C, C−Pt, and Pt−O at distances of 1.49, 1.40, 1.98, and 2.02 Å, respectively. The calculated energy barrier is about 0.57 eV and the reaction energy is 0.4 eV. The next step through a transition state (V) in which a free CO$_2$ molecule is produced with nearly no barrier. After the first CO$_2$ desorbs from the catalyst, there is an isolated oxygen atom on Pt. Subsequently, a second CO comes to coadsorb on Pt with the O atom (VII), and the reaction between CO and O is also stepwise. First, an intermediate (IX) is produced through the transition state (VIII), with a small barrier of 0.35 eV and a large exothermicity of −1.79 eV. A bent CO$_2$ intermediate is bound to the Pt atom with the O−Pt and C−Pt distances of 2.10 and 2.05 Å, respectively. Finally, the desorption of the CO$_2$ species requires an energy barrier of 0.94 eV, which is considered as the rate-determining step. It should be noted that the Pt atom is always pulled somewhat away from its original position during the process of oxidation, suggesting that the Pt atom on nondoped CeO$_2$(111) might not be very stable during the reaction.

On the Pt/Ga−CeO$_2$−O$_V$ SAC, however, CO oxidation begins with an O$_2$ molecule adsorption at the O$_V$ site with a CO species bound to the Pt atom (II, Figure 5). Different from the case of Pt/CeO$_2$, the generation of CO$_2$ requires a

relatively low energy barrier of 0.51 eV with an exothermicity of −1.71 eV. The MvK mechanism on Pt/Ga−CeO$_2$ is different from that in Figure 4, which is much more complex. In the transition state (III), the formed C−O bond has a length of about 1.97 Å. After reaction, a linear CO$_2$ species is physically adsorbed at the Pt atom (IV) with the adsorption energy of −0.46 eV. The desorption of the CO$_2$ product completes the catalytic cycle. Importantly, the Pt atom always remains in the initial position throughout the CO oxidation process, implying a very stable SAC. Compared to that (0.94 eV) for the bare CeO$_2$-supported Pt atoms, the overall energy barrier for the rate-determining step is reduced to 0.51 eV, indicating a better catalytic performance of the Pt atom supported on Ga-doped CeO$_2$. It is also found that such an energy barrier of CO oxidation on Pt/Ga−CeO$_2$ is quite close to that (0.48 eV) on Pt/CeO$_2$(110) with water participation, which follows a similar MvK mechanism.[39] The energy barrier of CO oxidation on Pt/Ga−CeO$_2$ is also much lower than that on Pt/FeO$_x$ (0.79 eV).[11]

It is thus concluded based on the DFT calculations that the Ga doping of CeO$_2$ leads to not only stronger Pt binding but also the facile generation of an oxygen vacancy nearby the Pt active site. The O$_2$ molecule can be efficiently activated by this O$_V$ site and then reacts with the adsorbed CO species on the single Pt atom, resulting in a lower energy barrier and a different reaction mechanism for CO oxidation.

3.5. Experimental Evidence. To verify the above theoretical prediction, we have carried out experimental studies on the Pt/CeO$_2$ and Pt/Ga−CeO$_2$ catalysts that are prepared using a similar procedure. We first performed CO oxidation monitored by DRIFTS on the Pt/CeO$_2$ and Pt/Ga−CeO$_2$ catalysts to understand the properties of the Pt species. The CO adsorption and desorption behavior on the Pt/CeO$_2$
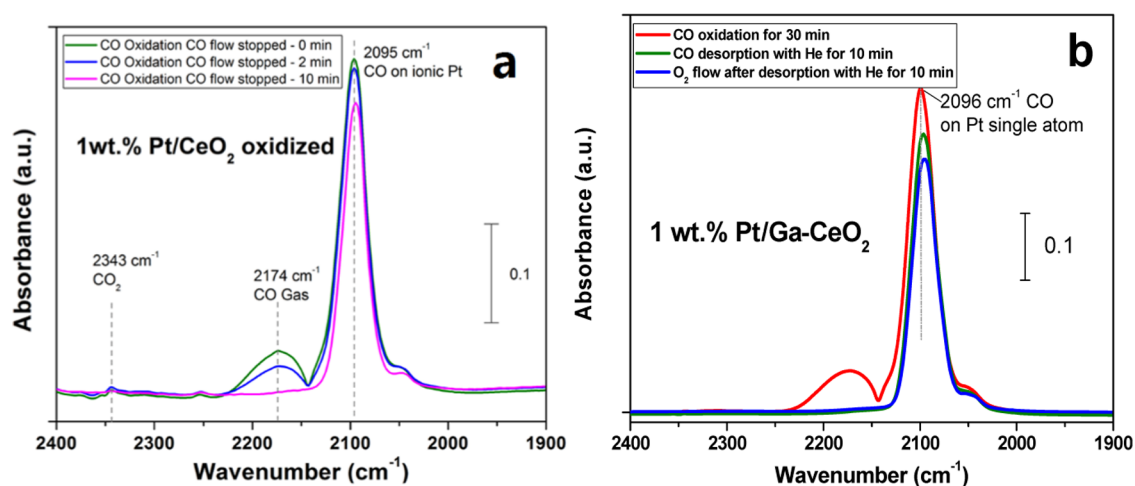
Figure 6. CO adsorption monitored by DRIFTS during CO oxidation and desorption at 125 °C for (a) Pt/CeO$_2$ single-atom catalyst (1 wt % Pt) and (b) Pt/Ga−CeO$_2$ (1 wt % Pt, Pt/Ga atomic ratio = 1). These spectra show that the Pt site on Pt/Ga−CeO$_2$ and Pt/CeO$_2$ is similar and both of them are Pt single atoms.
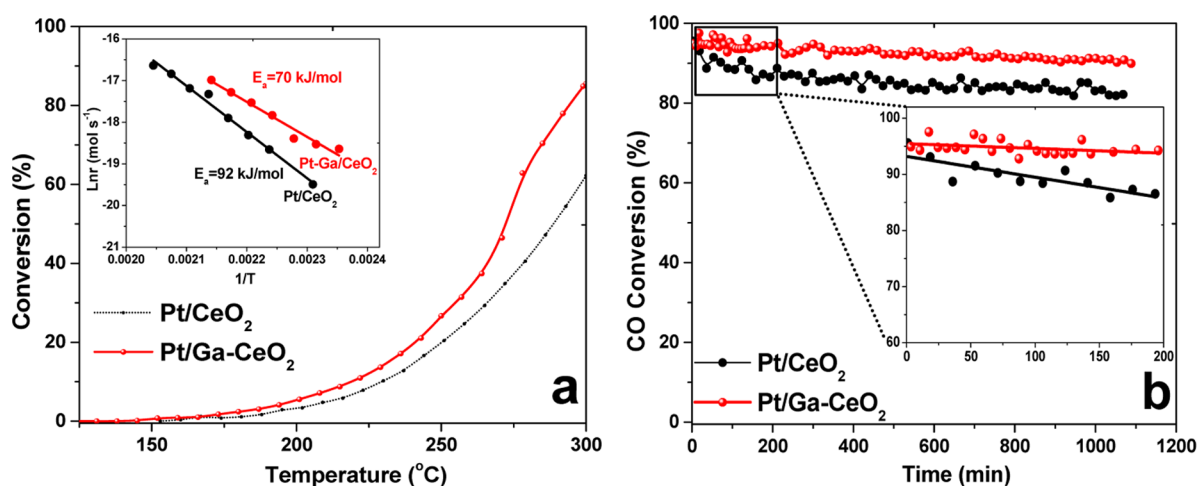
Figure 7. (a) Light-off curves and Arrhenius plots for Pt/CeO$_2$ and Pt/Ga−CeO$_2$ catalysts in CO oxidation (reaction conditions: [CO] = 1.9%, [O$_2$] = 1.3% balanced with helium). GHSV: 77 500 mL/(g$_{cat}$ h). Temperature ramp: 2 °C/min. (b) CO conversion as a function of time on stream for the atomically dispersed Pt/CeO$_2$ and Pt/Ga−CeO$_2$ catalysts. To achieve an initial CO conversion of ca. 95%, Pt/CeO$_2$ was tested at 337 °C and Pt/Ga−CeO$_2$ was tested at 319 °C (the activity of Pt/Ga−CeO$_2$ was also tested at 337 °C (100% CO conversion, Figure S2 in the Supporting Information), whereas no deactivation was found in 20 h). All the samples contain 1 wt % Pt. Pt/CeO$_2$ and Pt/Ga−CeO$_2$ were prepared by incipient wetness impregnation with CeO$_2$ (both catalysts were calcined in air at 800 °C for 12 h).

SAC has been studied in our previous work (Figure 6a).[18] For the Pt/Ga−CeO$_2$ SAC, the catalyst was pretreated in 10% O$_2$/He at 300 °C for 30 min, followed by decreasing the temperature to 125 °C. Then, CO/O$_2$ flow was switched on and the spectra were collected. As can be seen in Figure 6b, a peak at 2096 cm^{-1} is seen and the peak persists in flowing He or O$_2$ (i.e., stop the flow of CO and switch to flow of He or O$_2$). Based on the assignment in our previous work (Figure 6a),[18] the peak at 2096 cm^{-1} is assigned to the CO adsorbed on single Pt sites rather than on Pt nanoclusters because the frequencies of CO on Pt clusters, if present, would have been below 2080 cm^{-1}. Hence, the Pt/Ga−CeO$_2$ catalyst consists of atomically dispersed Pt sites under the reaction conditions used in this work.

We then performed CO oxidation over pure CeO$_2$, Ga−CeO$_2$, atomically dispersed Pt/CeO$_2$, and Pt/Ga−CeO$_2$ catalysts. Ga−CeO$_2$ shows a similar CO oxidation behavior as the CeO$_2$ support, both of which showed little activity

(Figure S1 in the Supporting Information). The light-off curves of the two catalysts in CO oxidation are shown in Figure 7a. Pt/Ga−CeO$_2$ shows higher reactivity than Pt/CeO$_2$ catalyst, which is in agreement with our DFT predictions (see energy barriers in Figures 4 and 5). Furthermore, the apparent activation energy (E_a) of the two catalysts for the reaction was determined from the temperature dependence (inset, Figure 7a). The E_a on Pt/CeO$_2$ is found to be 0.95 eV, which agrees well with our DFT result (0.94 eV). The experimental E_a of CO oxidation on Pt/Ga−CeO$_2$ is 0.73 eV, which is 0.22 eV higher than that calculated by DFT. The difference in the energy barriers between the DFT and the experiment might be caused by the nonuniform distribution of atomic Pt on the catalyst such that a portion of Pt atoms are not associated with Ga atoms.

The stability of the Pt/CeO$_2$ and Pt/Ga−CeO$_2$ SACs in CO oxidation was tested at an initial CO conversion of ca. 95%. The similar initial CO conversion provides similar CO partial

pressure that produces similar ripening effect because of the interaction between CO and Pt. The CO conversion of the two catalysts as a function of time on stream is shown in Figure 7b. It is seen that both Pt/Ga−CeO$_2$ and Pt/CeO$_2$ SACs underwent slight deactivation during the 20 h run under this condition. However, from the first 3 h run (Figure 7b, inset), the Pt/Ga−CeO$_2$ catalyst shows a lower deactivation rate than Pt/CeO$_2$, indicating that the former is more stable in CO oxidation. Therefore, one can conclude that doping of Ga into Pt/CeO$_2$ SAC is beneficial to the catalyst's stability. This is consistent with our DFT calculation that the Pt/Ga−CeO$_2$ SAC shows a higher binding energy of Pt than the Pt/CeO$_2$ SAC (Table 1). The DFT calculations show that adding Ga increases the Pt-support binding energy. A higher binding energy would suggest that Pt would have increased the stability at higher temperatures. This may explain the lower deactivation rate in the first 3 h of the time on stream test for the Pt/Ga−CeO$_2$ catalyst.

Our DFT calculations show that the Ga dopant can decrease the adsorption energy of CO on the Pt single atoms while stabilizing the Pt atoms during CO oxidation at high temperatures. In our previous study, doping Sn into Pt/CeO$_2$ single-atom catalyst was also found to decrease the adsorption energy of another molecule (i.e., C$_2$H$_4$) on Pt.[15] The present experimental results on CO oxidation indicate that the Pt/Ga−CeO$_2$ SAC shows a higher reactivity than Pt/CeO$_2$ due to the facile creation of an oxygen vacancy near the active site. Especially, the properties of a Pt SAC can be tuned by adding a dopant metal atom to the ceria support, and this finding will help in the broader utilization of stable SACs for other chemical conversions.

4. CONCLUSIONS

In this work, the stability and CO oxidation activity of Pt SACs supported on CeO$_2$(111) and Ga-doped CeO$_2$(111) were investigated by DFT and experiments. Our DFT calculations show that the binding energy of the Pt atom to the support is significantly increased with Ga doping, suggesting that the Pt atom is more stable at high temperatures. Further calculations show that an oxygen vacancy can be generated near the Pt site with Ga doping. From the kinetic studies, it is shown that the energy barrier of CO oxidation is reduced on the Pt/Ga−CeO$_2$−O$_V$ SAC, highlighting the benefit of support doping. Our experimental results agree well with these theoretical predictions and the combination of theory and experiment sheds valuable light on the importance of doping a heterometal on atomically dispersed Pt/CeO$_2$ single-atom catalysts.

■ ASSOCIATED CONTENT

ⓢ Supporting Information

The Supporting Information is available free of charge on the ACS Publications website at DOI: 10.1021/acs.jpcc.8b05815.

> Light off curves of CO oxidation on CeO$_2$ and Ga−CeO$_2$ showing the similar reactivity; CO conversion as a function of time on stream for the atomically dispersed Pt/CeO$_2$ and Pt/Ga−CeO$_2$ catalysts carried out at 337 °C (PDF)

■ AUTHOR INFORMATION

Corresponding Authors

*E-mail: hfxiong@unm.edu (H.X.).
*E-mail: slin@fzu.edu.cn (S.L.).
*E-mail: datye@unm.edu (A.K.D.).
*E-mail: hguo@unm.edu (H.G.).

ORCID ◉

Yingxin Feng: 0000-0002-5817-4391
Haifeng Xiong: 0000-0002-3964-4677
Xavier Isidro Pereira Hernandez: 0000-0002-7020-0011
Sen Lin: 0000-0002-2288-5415
Hua Guo: 0000-0001-9901-053X

Notes

The authors declare no competing financial interest.

■ ACKNOWLEDGMENTS

■ REFERENCES

(1) Wei, H.; Liu, X.; Wang, A.; Zhang, L.; Qiao, B.; Yang, X.; Huang, Y.; Miao, S.; Liu, J.; Zhang, T. FeO$_x$-Supported Platinum Single-Atom and Pseudo-Single-Atom Catalysts for Chemoselective Hydrogenation of Functionalized Nitroarenes. *Nat. Commun.* **2014**, *5*, No. 5634.

(2) Peterson, E. J.; DeLaRiva, A. T.; Lin, S.; Johnson, R. S.; Guo, H.; Miller, J. T.; Hun Kwak, J.; Peden, C. H. F.; Kiefer, B.; Allard, L. F.; et al. Low-Temperature Carbon Monoxide Oxidation Catalysed by Regenerable Atomically Dispersed Palladium on Alumina. *Nat. Commun.* **2014**, *5*, No. 4885.

(3) Lin, J.; Wang, A.; Qiao, B.; Liu, X.; Yang, X.; Wang, X.; Liang, J.; Li, J.; Liu, J.; Zhang, T. Remarkable Performance of Ir$_1$/FeO$_x$ Single-Atom Catalyst in Water Gas Shift Reaction. *J. Am. Chem. Soc.* **2013**, *135*, 15314−15317.

(4) Yang, X.-F.; Wang, A.; Qiao, B.; Li, J.; Liu, J.; Zhang, T. Single-Atom Catalysts: A New Frontier in Heterogeneous Catalysis. *Acc. Chem. Res.* **2013**, *46*, 1740−1748.

(5) Lin, S.; Ye, X.; Johnson, R. S.; Guo, H. First-Principles Investigations of Metal (Cu, Ag, Au, Pt, Rh, Pd, Fe, Co, and Ir) Doped Hexagonal Boron Nitride Nanosheets: Stability and Catalysis of CO Oxidation. *J. Phys. Chem. C* **2013**, *117*, 17319−17326.

(6) Feng, Y.; Zhou, L.; Wan, Q.; Lin, S.; Guo, H. Selective Hydrogenation of 1,3-Butadiene Catalyzed by a Single Pd Atom Anchored on Graphene: The Importance of Dynamics. *Chem. Sci.* **2018**, *9*, 5890−5896.

(7) Huang, C.; Ye, X.; Chen, C.; Lin, S.; Xie, D. A Computational Investigation of CO Oxidation on Ruthenium-Embedded Hexagonal Boron Nitride Nanosheet. *Comput. Theor. Chem.* **2013**, *1011*, 5−10.

(8) Wang, S.; Feng, Y.; Lin, S.; Guo, H. Phosphomolybdic Acid Supported Atomically Dispersed Transition Metal Atoms (M = Fe, Co, Ni, Cu, Ru, Rh, Pd, Ag, Os, Ir, Pt, and Au): Stable Single Atom Catalysts Studied by Density Functional Theory. *RSC Adv.* **2017**, *7*, 24925−24932.

(9) Song, W.; Hensen, E. J. M. Mechanistic Aspects of the Water−Gas Shift Reaction on Isolated and Clustered Au Atoms on CeO$_2$(110): A Density Functional Theory Study. *ACS Catal.* **2014**, *4*, 1885−1892.

(10) Liu, J. Catalysis by Supported Single Metal Atoms. *ACS Catal.* **2017**, 7, 34−59.

(11) Qiao, B.; Wang, A.; Yang, X.; Allard, L. F.; Jiang, Z.; Cui, Y.; Liu, J.; Li, J.; Zhang, T. Single-Atom Catalysis of CO Oxidation Using Pt_1/FeO_x. *Nat. Chem.* **2011**, 3, 634.

(12) Kwak, J. H.; Hu, J.; Mei, D.; Yi, C.-W.; Kim, D. H.; Peden, C. H. F.; Allard, L. F.; Szanyi, J. Coordinatively Unsaturated Al^{3+} Centers as Binding Sites for Active Catalyst Phases of Platinum on γ-Al_2O_3. *Science* **2009**, 325, 1670−1673.

(13) Li, W. Z.; Kovarik, L.; Mei, D.; Liu, J.; Wang, Y.; Peden, C. H. Stable Platinum Nanoparticles on Specific $MgAl_2O_4$ Spinel Facets at High Temperatures in Oxidizing Atmospheres. *Nat. Commun.* **2013**, 4, No. 2481.

(14) Johns, T. R.; Gaudet, J. R.; Peterson, E. J.; Miller, J. T.; Stach, E. A.; Kim, C. H.; Balogh, M. P.; Datye, A. K. Microstructure of Bimetallic PtPd Catalysts under Oxidizing Conditions. *ChemCatChem* **2013**, 5, 2636−2645.

(15) Xiong, H.; Lin, S.; Goetze, J.; Pletcher, P.; Guo, H.; Kovarik, L.; Artyushkova, K.; Weckhuysen, B. M.; Datye, A. K. Thermally Stable and Regenerable Platinum−Tin Clusters for Propane Dehydrogenation Prepared by Atom Trapping on Ceria. *Angew. Chem., Int. Ed.* **2017**, 56, 8986−8991.

(16) Uchiyama, T.; Yoshida, H.; Kuwauchi, Y.; Ichikawa, S.; Shimada, S.; Haruta, M.; Takeda, S. Systematic Morphology Changes of Gold Nanoparticles Supported on CeO_2 During CO Oxidation. *Angew. Chem.* **2011**, 123, 10339−10342.

(17) Paier, J.; Penschke, C.; Sauer, J. Oxygen Defects and Surface Chemistry of Ceria: Quantum Chemical Studies Compared to Experiment. *Chem. Rev.* **2013**, 113, 3949−3985.

(18) Jones, J.; Xiong, H.; DeLaRiva, A. T.; Peterson, E. J.; Pham, H.; Challa, S. R.; Qi, G.; Oh, S.; Wiebenga, M. H.; Pereira Hernández, X. I.; et al. Thermally Stable Single-Atom Platinum-on-Ceria Catalysts Via Atom Trapping. *Science* **2016**, 353, 150−154.

(19) Nie, L.; Mei, D.; Xiong, H.; Peng, B.; Ren, Z.; Pereira Hernández, X. I.; DeLaRiva, A.; Wang, M.; Engelhard, M. H.; Kovarik, L.; et al. Activation of Surface Lattice Oxygen in Single-Atom Pt/CeO_2 for Low-Temperature CO Oxidation. *Science* **2017**, 358, 1419−1423.

(20) Kresse, G.; Furthmüller, J. Efficient Iterative Schemes for Ab Initio Total-Energy Calculations Using a Plane-Wave Basis Set. *Phys. Rev. B* **1996**, 54, 11169−11186.

(21) Kresse, G.; Furthmüller, J. Efficiency of Ab-Initio Total Energy Calculations for Metals and Semiconductors Using a Plane-Wave Basis Set. *Comput. Mater. Sci.* **1996**, 6, 15−50.

(22) Kresse, G.; Hafner, J. Ab Initiomolecular Dynamics for Liquid Metals. *Phys. Rev. B* **1993**, 47, 558−561.

(23) Huang, M.; Fabris, S. CO Adsorption and Oxidation on Ceria Surfaces from DFT+U Calculations. *J. Phys. Chem. C* **2008**, 112, 8643−8648.

(24) Liu, J.-C.; Wang, Y.-G.; Li, J. Toward Rational Design of Oxide-Supported Single-Atom Catalysts: Atomic Dispersion of Gold on Ceria. *J. Am. Chem. Soc.* **2017**, 139, 6190−6199.

(25) Kim, K.; Yoo, J. D.; Lee, S.; Bae, M.; Bae, J.; Jung, W.; Han, J. W. A Simple Descriptor to Rapidly Screen CO Oxidation Activity on Rare-Earth Metal-Doped CeO_2: From Experiment to First-Principles. *ACS Appl. Mater. Interfaces* **2017**, 9, 15449−15458.

(26) Kresse, G.; Joubert, D. From Ultrasoft Pseudopotentials to the Projector Augmented-Wave Method. *Phys. Rev. B* **1999**, 59, 1758−1775.

(27) Branda, M. M.; Hernández, N. C.; Sanz, J. F.; Illas, F. Density Functional Theory Study of the Interaction of Cu, Ag, and Au Atoms with the Regular CeO_2 (111) Surface. *J. Phys. Chem. C* **2010**, 114, 1934−1941.

(28) Gerward, L.; Staun Olsen, J.; Petit, L.; Vaitheeswaran, G.; Kanchana, V.; Svane, A. Bulk Modulus of CeO_2 and PrO_2—an Experimental and Theoretical Study. *J. Alloys Compd.* **2005**, 400, 56−61.

(29) Henkelman, G.; Uberuaga, B. P.; Jónsson, H. A Climbing Image Nudged Elastic Band Method for Finding Saddle Points and Minimum Energy Paths. *J. Chem. Phys.* **2000**, 113, 9901−9904.

(30) Nolan, M.; Grigoleit, S.; Sayle, D. C.; Parker, S. C.; Watson, G. W. Density Functional Theory Studies of the Structure and Electronic Structure of Pure and Defective Low Index Surfaces of Ceria. *Surf. Sci.* **2005**, 576, 217−229.

(31) Dvořák, F.; Farnesi Camellone, M.; Tovt, A.; Tran, N.-D.; Negreiros, F. R.; Vorokhta, M.; Skála, T.; Matolínová, I.; Mysliveček, J.; Matolín, V.; et al. Creating Single-Atom Pt-Ceria Catalysts by Surface Step Decoration. *Nat. Commun.* **2016**, 7, No. 10801.

(32) Bruix, A.; Neyman, K. M.; Illas, F. Adsorption, Oxidation State, and Diffusion of Pt Atoms on the $CeO_2(111)$ Surface. *J. Phys. Chem. C* **2010**, 114, 14202−14207.

(33) Kehoe, A. B.; Scanlon, D. O.; Watson, G. W. Role of Lattice Distortions in the Oxygen Storage Capacity of Divalently Doped CeO_2. *Chem. Mater.* **2011**, 23, 4464−4468.

(34) Wang, H.-F.; Gong, X.-Q.; Guo, Y.-L.; Guo, Y.; Lu, G. Z.; Hu, P. A Model to Understand the Oxygen Vacancy Formation in Zr-Doped CeO_2: Electrostatic Interaction and Structural Relaxation. *J. Phys. Chem. C* **2009**, 113, 10229−10232.

(35) Tang, Y.; Wang, Y.-G.; Li, J. Theoretical Investigations of $Pt_1@CeO_2$ Single-Atom Catalyst for CO Oxidation. *J. Phys. Chem. C* **2017**, 121, 11281−11289.

(36) Aydin, C.; Lu, J.; Browning, N. D.; Gates, B. C. A "Smart" Catalyst: Sinter-Resistant Supported Iridium Clusters Visualized with Electron Microscopy. *Angew. Chem., Int. Ed.* **2012**, 51, 5929−5934.

(37) Chen, Y.; Huang, Z.; Ma, Z.; Chen, J.; Tang, X. Fabrication, Characterization, and Stability of Supported Single-Atom Catalysts. *Catal. Sci. Technol.* **2017**, 7, 4250−4258.

(38) Campbell, C. T.; Sellers, J. R. V. Anchored Metal Nanoparticles: Effects of Support and Size on Their Energy, Sintering Resistance and Reactivity. *Faraday Discuss.* **2013**, 162, 9−30.

(39) Wang, C.; Gu, X.-K.; Yan, H.; Lin, Y.; Li, J.; Liu, D.; Li, W.-X.; Lu, J. Water-Mediated Mars−Van Krevelen Mechanism for CO Oxidation on Ceria-Supported Single-Atom Pt_1 Catalyst. *ACS Catal.* **2017**, 7, 887−891.

(40) Royer, S.; Duprez, D. Catalytic Oxidation of Carbon Monoxide over Transition Metal Oxides. *ChemCatChem* **2011**, 3, 24−65.

(41) Chen, M. S.; Cai, Y.; Yan, Z.; Gath, K. K.; Axnanda, S.; Goodman, D. W. Highly Active Surfaces for CO Oxidation on Rh, Pd, and Pt. *Surf. Sci.* **2007**, 601, 5326−5331.

(42) Yu, M.-a.; Feng, Y.; Gao, L.; Lin, S. Phosphomolybdic Acid Supported Single-Metal-Atom Catalysis in CO Oxidation: First-Principles Calculations. *Phys. Chem. Chem. Phys.* **2018**, 20, 20661−20668.

(43) Lin, S.; Huang, J.; Gao, X. A Cu(111) Supported h-BN Nanosheet: A Potential Low-Cost and High-Performance Catalyst for CO Oxidation. *Phys. Chem. Chem. Phys.* **2015**, 17, 22097−22105.

(44) Lin, S.; Ye, X.; Huang, J. Can Metal-Free Silicon-Doped Hexagonal Boron Nitride Nanosheets and Nanotubes Exhibit Activity toward CO Oxidation? *Phys. Chem. Chem. Phys.* **2015**, 17, 888−895.

(45) Li, F.; Li, Y.; Zeng, X. C.; Chen, Z. Exploration of High-Performance Single-Atom Catalysts on Support M_1/FeO_x for CO Oxidation Via Computational Study. *ACS Catal.* **2015**, 5, 544−552.